THE GEOLOGICAL SOCIETY OF AMERICA®

Meishucun phosphorite succession (SW China) records redox changes of the early Cambrian ocean

Ze-Rui Ray Liu[1†] and Mei-Fu Zhou[1,2†]

[1]*Department of Earth Sciences, University of Hong Kong, Pokfulam Road, Hong Kong, China*

[2]*State Key Laboratory of Ore Deposit Geochemistry, Institute of Geochemistry, Chinese Academy of Sciences, Guiyang 550081, China*

ABSTRACT

Two early Cambrian phosphorite units from the Meishucun section, SW China, were investigated to decipher the mechanism of phosphogenesis and to understand the redox states of the early Cambrian ocean. Rocks from the lower unit contain abundant cyanobacterial-like microfossils and radial francolite aggregates, and they have oolitic textures, a negative $\delta^{13}C_{carb}$ shift, and kerogen-like rare earth element (REE) patterns. These rocks were derived from degradation of organisms and were subsequently reworked by high-energy water. In contrast, rocks from the upper unit are dominated by stumpy francolite and have high Zn (40–185 ppm) and Pb (15–845 ppm) contents and seawater-like REE patterns, indicating that P adsorption and regeneration were mediated by Fe-(oxyhydr)oxides. Phosphorites in this unit were episodically exposed above the wave base and are characterized by bedding structures. Rocks from the lower unit have low V (3–18 ppm) and Cr (7–20 ppm) contents and negative $\delta^{97/95}$Mo values, clearly suggesting that the ambient water was oxygenated due to proliferation of cyanobacteria. The upper unit must have formed near a Fe-redox boundary in sediments that allowed the transformation between Fe^{3+} and Fe^{2+}, consistent with high V (18–55 ppm) and Cr (20–62 ppm) contents, and positive $\delta^{97/95}$Mo values in the unit. The oceanic reduction may be attributed to the ca. 535 Ma volcanism and hydrothermal venting in the basin. Similar compositions of phosphorites from the lower unit and equivalents elsewhere indicate that the early Cambrian phosphogenesis was controlled mainly by proliferation of primary producers. Given that shallow water above the wave base can be well mixed and in equilibrium with atmospheric oxygen, the subsequent reducing environment in the ocean recorded in the upper unit may have been a global phenomenon.

INTRODUCTION

The diversification of eukaryotes and emergence of skeletal animals at the beginning of Cambrian (542–520 Ma) indicate that oxygen of seawaters had risen beyond the minimum requirements for animal life at that time (Anbar and Knoll, 2002; Chen et al., 2015; Sperling et al., 2013). Recent biological and isotopic studies of black shales further suggest that most bottom waters in the early Cambrian ocean were well oxygenated at ca. 521 Ma (Chen et al., 2015; Zhou and Jiang, 2009). In contrast, the enrichment of redox-sensitive elements in marine sediments has been interpreted to indicate that seawaters, particularly bottom waters, were anoxic or even euxinic due to the accumulation and subsequent anaerobic oxidation of organic matter (Jiang et al., 2006; Schroder and Grotzinger, 2007). The shallow waters of the early Cambrian ocean are also thought to have been oxygen deficient due to the transgressive upward movement of the anoxic bottom waters (Kimura and Watanabe, 2001). There is no consensus regarding the redox state and circulation patterns of the early Cambrian ocean, which impedes our understanding of the evolution of life at that time.

Early Cambrian phosphorus sedimentary successions are widely distributed, especially in central and southeastern Asia and Australia (Cook and Shergold, 1986; Papineau, 2010). Authigenic phosphate-bearing sedimentary rocks contain information about redox states and chemical compositions of the shallow ocean. For instance, abundant cyanobacteria in phosphorites from the Paleoproterozoic Aravalli Supergroup, India (Papineau et al., 2013), and the Neoproterozoic Doushantuo Formation, South China (She et al., 2013, 2014), suggest that phosphogenesis was likely linked to cyanobacteria blooming and subsequent oxygen elevation; most Ediacaran–Cambrian granular phosphorites are depleted in heavy rare earth elements (HREEs), contrary to their modern counterparts, indicative of low HREE concentrations in the Ediacaran–Cambrian ocean (Ilyin, 1998).

The Yangtze platform at the transition from the Precambrian to Cambrian is considered to be one of the largest depositional sites of phosphorites (Fig. 1; Ilyin, 1998). The early Cambrian phosphorite succession in the Meishucun area, Yunnan Province, is composed of two units separated by an ~1.6-m-thick tuff layer with a zircon U-Pb age of 535.2 ± 1.7 Ma (Zhu et al., 2009). Although it is known that these two units have different petrological and geochemical features (Shields and Stille, 2001; Wen et al., 2011), the significance of these differences for the understanding of redox states of the ocean is not well documented. In this paper, we describe the petrography of these two units and report new findings that are used to constrain their origins. On the basis of the new data set, we propose that the two phosphorite units were formed under conditions that have significant implications for environmental change during the early Cambrian.

GEOLOGICAL BACKGROUND

The South China block, including the Yangtze block to the northwest and the Cathaysia block to the southeast, is bounded by the Mesozoic Qinling-Dabie-Sulu orogenic belt to the north, the Mesozoic–Cenozoic Longmenshan orogenic belt to the northwest, the Indochina block to the southwest, and the Cenozoic continental slope of the East China and South China Seas to the southeast (Fig. 1; Z.-X. Li et al., 1995; Zhao et al., 2011). The late Neoproterozoic to early Cambrian strata in the Cathaysia block are dominated by continental clastic rocks, whereas the Yangtze block is covered by Cryogenian

†Zhou, corresponding author—mfzhou@hkucc.hku.hk; Liu—guayu@126.com.

GSA Bulletin; November/December 2017; v. 129; no. 11/12; p. 1554–1567; https://doi.org/10.1130/B31612.1; 9 figures; Data Repository item 2017220; published online 7 July 2017.

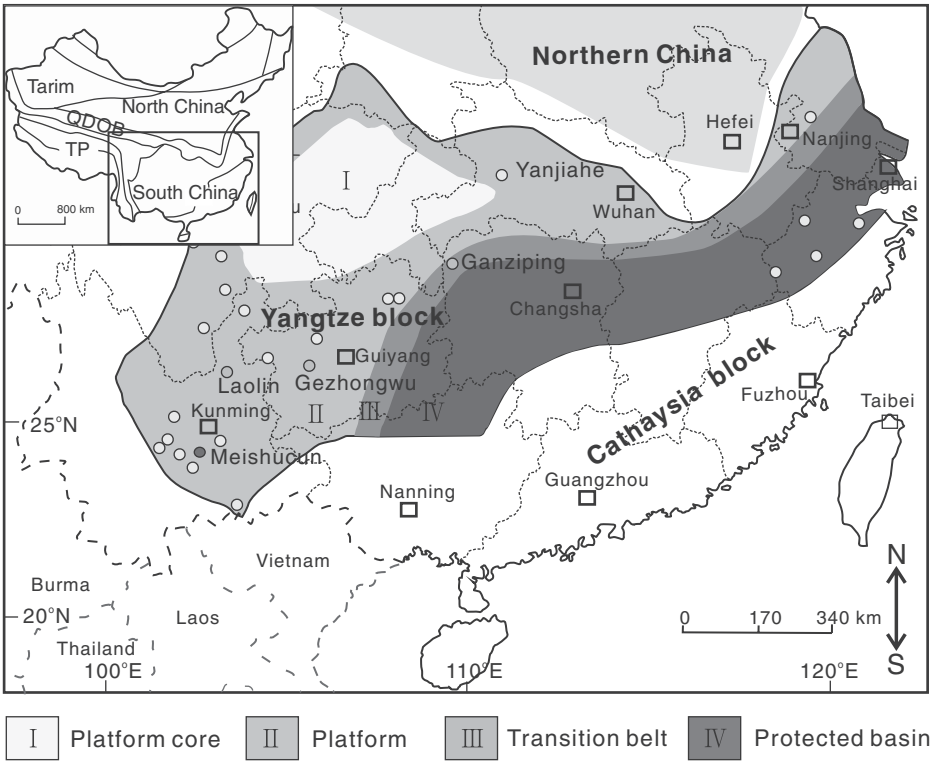

Figure 1. Simplified paleogeographic map of the Yangtze block during the Ediacaran-Cambrian transition, showing the four major facies under consideration (modified from Steiner et al., 2001; Wen et al., 2015). Circles represent the major outcrops of early Cambrian phosphorite successions. QDOB—Qinling-Dabie orogenic belt; TP—Tibetan Plateau.

continental clastic rocks and Ediacaran to Cambrian carbonates, phosphorites, and carbonaceous shales (Wang and Zhou, 2012; Yan et al., 2003; Yao et al., 2014).

Stratigraphic units across the Ediacaran-Cambrian transition in the Yangtze block were deposited in environments including platform, transitional belt, and protected basin (Fig. 1; Steiner et al., 2001; Wen et al., 2015). These units include the Zhujiaqing, Gezhongwu, Yanjiahe, Maidiping, and Liuchapo Formations in different locations (Guo et al., 2007; Ishikawa et al., 2008; Li et al., 2013; Luo et al., 1984; Wen et al., 2015). The Zhujiaqing Formation in the southwestern Yangtze block is dominated by algal dolostone and phosphorite (Xing and Luo, 1984). The underlain Ediacaran Dengying Formation consists of dolostone with cherty layers, whereas the overlain Shiyantou Formation is composed of black shale and dolostone (Li et al., 2009; Wen et al., 2011).

In Meishucun, phosphorites of the early Cambrian Fortunian stage are hosted in the Zhongyicun Member of the Zhujiaqing Formation (Pašava et al., 2010). They lie on the southern limb of the Xiangtiaochong anticline with a gentle attitude. The stratigraphic succession in the Meishucun section consists of the Ediacaran Baiyanshao Member and the early Cambrian Xiaowaitoushan, Zhongyicun, Dahai, and Shiyantou Members of the Zhujiaqing Formation (Fig. 2; supplementary Fig. A1[1]), and it was one of the global stratotype section and point candidates for the Precambrian-Cambrian boundary (Xing and Luo, 1984). The Baiyanshao and Xiaowaitoushan Members are dominated by algal dolostones with well-preserved cross-bedding structures (Fig. 2). The uppermost part of the Xiaowaitoushan Member contains phosphorus nodules ranging from 0.1 to 2 cm in size and is used to mark the boundary between the Xiaowaitoushan and Zhongyicun Members. The Zhongyicun Member is dominated by dolomitic phosphorites with siliceous clasts, and it is divided into two units by a tuff layer (Shields and Stille, 2001; Wen et al., 2011). The lower unit contains abundant small shelly fossils of the *Anabarites–Protohertzina* assemblage. The upper unit and overlying Dahai Member have small shelly fossils of the *Paragloborilus–Siphogonuchites* assemblage (Wen et al., 2011; Xing and Luo, 1984).

[1]GSA Data Repository item 2017220, analytical methods, supplementary Figures A1–A7 and Table C1, is available at http://www.geosociety.org/datarepository/2017 or by request to editing@geosociety.org.

PETROGRAPHY

Dolostones and dolomitic phosphorites were collected from the Baiyanshao, Xiaowaitoushan, and Zhongyicun Members upward to the Dahai Member across the profile in Meishucun (Fig. 2).

Dolostones from the Baiyanshao, Xiaowaitoushan, and Dahai Members

These three members contain dolomite (>70 vol%), terrigenous clasts (~25 vol%), and collophanite (<5 vol%). Dolomite is coarse grained and mostly >100 μm in diameter. Angular to subrounded terrigenous clasts are mainly composed of quartz, feldspar, and mica. Granular collophanite grains contain trace amounts of carbonaceous matter (Fig. 3A).

Phosphorites from the Zhongyicun Member

Lower Unit

Phosphorites from this unit consist of >60 vol% collophanite, 20–30 vol% dolomite, 10–20 vol% terrigenous clasts, and small amounts of carbonaceous matter (Fig. 3B). Fossils in the lower unit include animal embryos, *Olivooides blandes*, *Protohertzina anabarica*, and coccoidal microfossils (Figs. 3C and 3E–3I). Terrigenous components are detrital quartz with rare feldspar and clay minerals, mainly subangular to subrounded (Figs. 3I and 3J). Collophanite grains generally show oolitic textures with long axes ranging from 100 to 350 μm (Figs. 3B and 3D). Their cores contain disseminated carbonaceous matter and remains of coccoidal microorganisms (4–15 μm in diameter; Fig. 3E) identified by Raman spectroscopy (bands at 1326 and 1612 cm^{-1}; see supplementary Fig. A2 [see footnote 1]). Observation under the scanning electron microscope (SEM) showed that francolite grains in coccoidal carbonaceous matter are tufted and range from 0.1 to 0.5 μm in size (Figs. 4A–4C), whereas those interstitial between coccoid forms are larger (1 μm) in size and radially aggregated (Fig. 4B). The crusts of oolitic grains show asymmetric or concentric zoning consisting of parallel columnar francolite grains ~1.5 μm in size (Fig. 4D). Collophanite

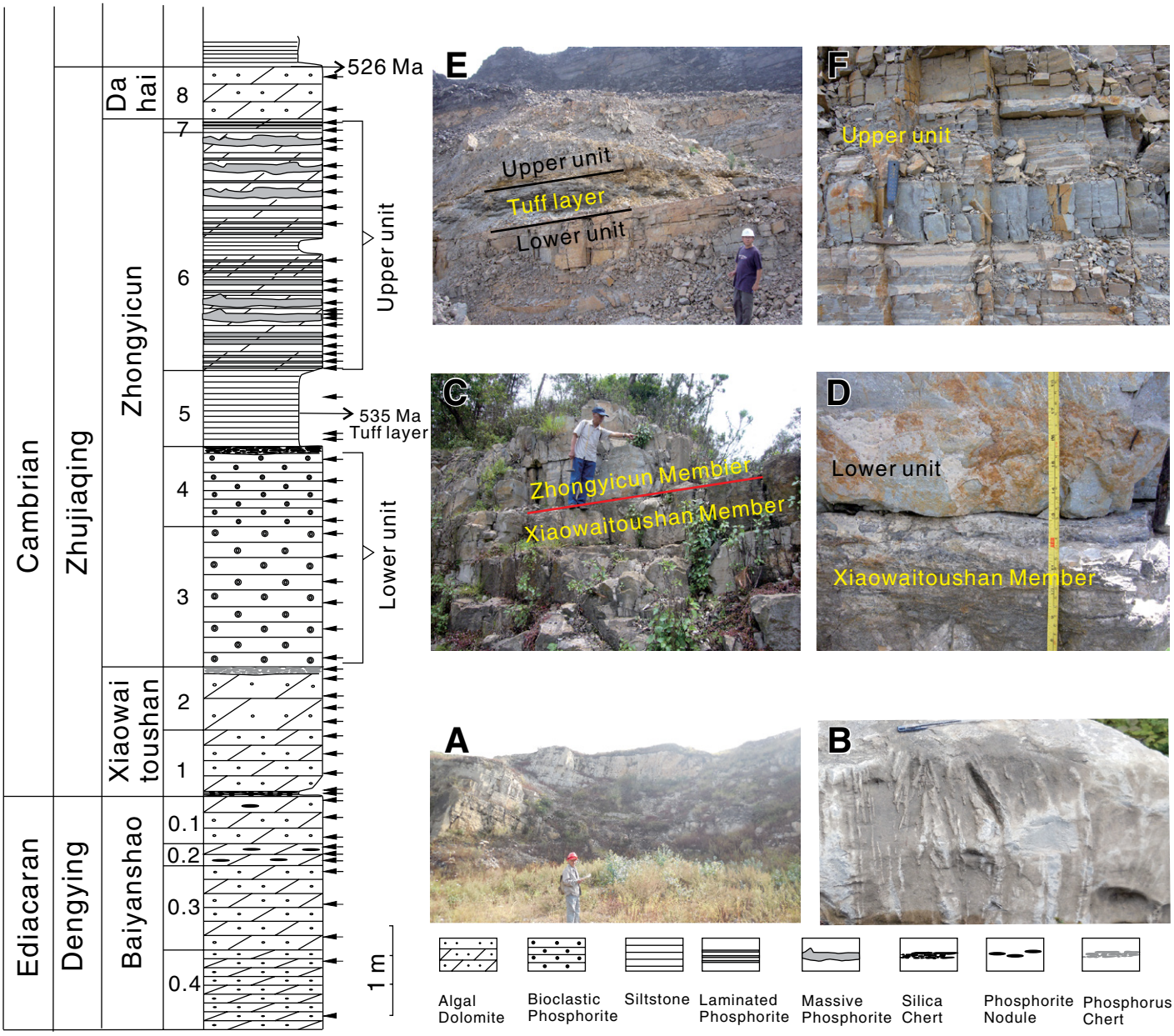

Figure 2. Integrated stratigraphy and field photos of the Dengying and Zhujiaqing formations in the Meishucun area, SW China: (A) Baiyanshao Member dolostones; (B) cross-bedding structure in the Baiyanshao Member; (C, D) Xiaowaitoushan dolostones and the lower unit of the Zhongyicun Member; and (E, F) tuff layer and bedded upper unit of the Zhongyicun Member. Arrows represent the sampling locations. Secondary ion mass spectrometry (SIMS) U-Pb zircon age of 535 Ma for the tuff layer in the middle Zhongyicun Member is from Zhu et al. (2009); SIMS U-Pb zircon age of 526 Ma for bentonites at the base of Shiyantou Formation is from Compston et al. (2008). The numbers to the left of the stratigraphic column refer to a subdivision of the members according to the lithology or thickness of the rock layers (Xing and Luo, 1984).

interclasts and terrigenous components are cemented by radially aggregated francolite and mosaic quartz (Fig. 4E). Clay minerals, goethite, and authigenic quartz occur in interspaces of collophanite grains (Figs. 4G–4I). Authigenic quartz contains francolite and rounded or rhombic pyrite grains (Figs. 4G and 4J–4L).

Upper Unit

The upper unit of the Zhongyicun Member is composed of alternating laminated and massive phosphorites. The laminated phosphorite is composed of dolomite (50–70 vol%), collophanite (20–30 vol%), and terrigenous clasts (10 vol%). Aligned collophanite occurs in the interstices between dolomite grains (Fig. 5A). Massive layers are dominated by densely packed and sand-sized granules (Fig. 5B). Oolitic textures are rare in granules (Fig. 5C). Francolite grains in collophanite granules and cements are mainly stumpy, although some are radially aggregated (Figs. 5E and 5F). Francolite

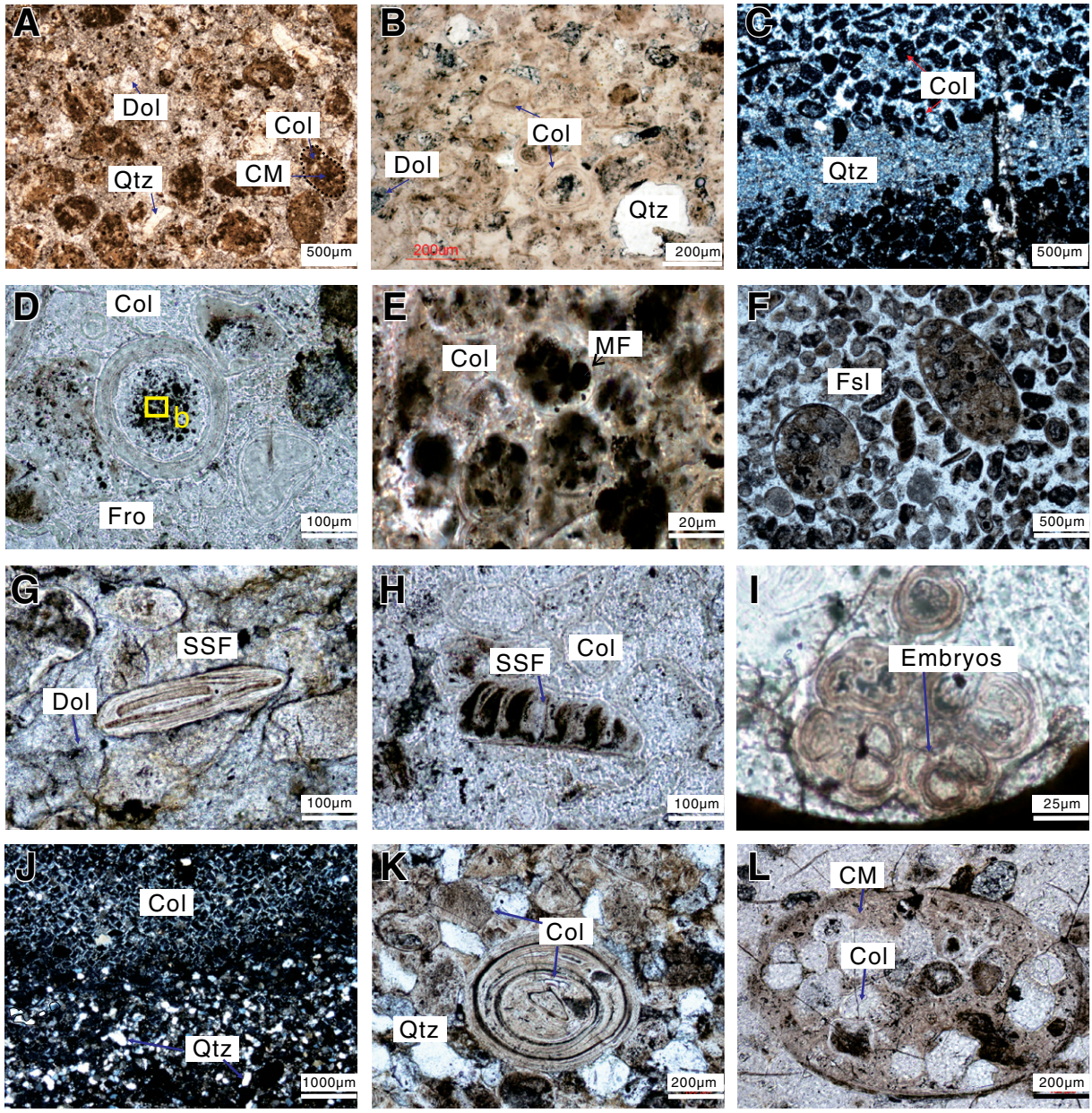

Figure 3. Microphotographs of the Zhujiaqing Formation: (A) Collophanite grains in the upper Xiaowaitoushan Member, (B) oolitic texture, (C) cherty layer atop the lower unit, (D, E) carbonaceous matter and Myxococcoides, (F–H) small shelly fossils: (F) *Olivooides blandes*, (G) *Eohalobia diandongensis*, (H) *Lapworthella rete*, (I) animal embryos, (J) density differentiation, (K) superimposed oolitic texture, and (L) large intraclast in the lower unit of phosphorite in Meishucun. CM—carbonaceous matter, Col—collophanite, Dol—dolomite, Fro—francolite, Fsl—fossils, MF—microfossils, Qtz—quartz, SSF—small shelly fossil.

grains on the surface of clay minerals are ~0.1 μm in size (Fig. 5G). Euhedral quartz crystals are embedded in large collophanite grains, and micron-size francolite crystals also occur within the quartz grains (Fig. 5H). Iron-rich oxides, which contain abundant P, S, Pb, and Zn, occur as small particles in the interspace of phosphate granules (Figs. 5I–5L).

GEOCHEMICAL FEATURES

In total, 58 samples were collected from a 25-m-thick interval that covers stratigraphic units from the upper Baiyanshao Member to the Dahai Member in Meishucun, SW China (24°43′50.7″N, 102°34′6.9″E). Whole-rock major- and trace-element, total organic carbon (TOC), and C and O isotope analyses were carried out, and the results are listed in supplementary Table C1 (see footnote 1).

Dolostones

Rocks from the Baiyanshao Member are dolomitic and have <2 wt% P_2O_5, <19 wt% SiO_2,

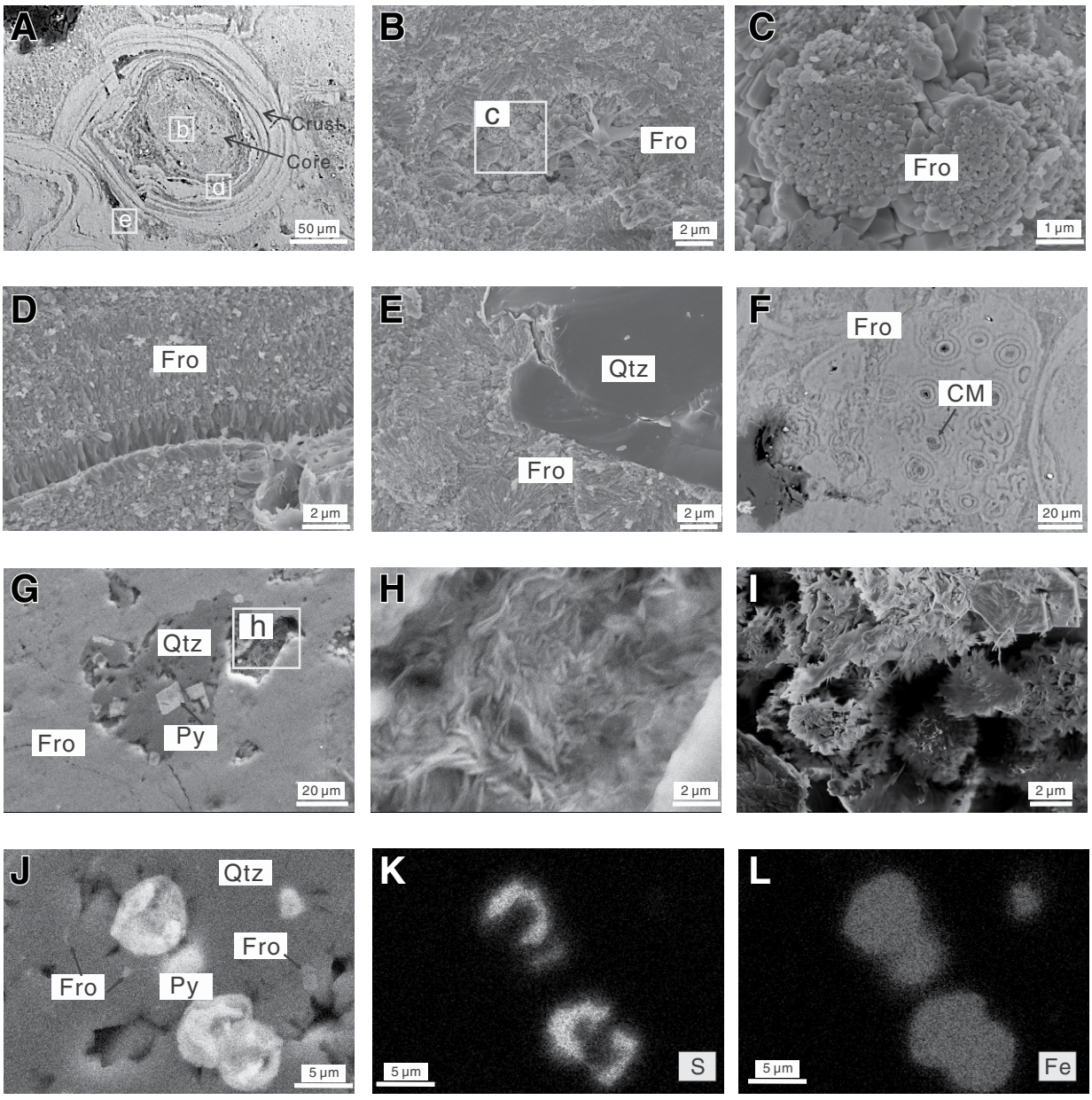

Figure 4. (A, F–H, J) Backscattered electron (BSE) images, (B–E, I) secondary electron images (SEIs), and (K, L) energy dispersive spectroscopy (EDS) spectra of the lower unit of phosphorite in Meishucun: (A) phosphatic granule with poriferous core and compact crust; (B–C) radially aggregated submicron-sized francolite crystals; (D) prismatic francolite crystals oriented perpendicular to the surface of granule; (E) radially aggregated francolite crystals in the cements; (F) francolites crystallized along microsized substrates; (G) rhombic pyrite; (H) sheet clay mineral; (I) goethite; (J, K) rounded pyrite and fine francolite in quartz; and (K) and (L) sulfur and iron distribution in area of (J). CM—carbonaceous matter, Fe—iron, Fro—francolite, Qtz—quartz, Py—pyrite, S—sulfur.

15–18 wt% MgO, 1.0–2.2 wt% Al_2O_3, and 0.1–1.3 wt% TOC. They have large ranges of Pb (5.4–98 ppm) and Zn (8.8–48 ppm). Their $\delta^{13}C_{carb}$, $\delta^{18}O_{carb}$, and $\delta^{13}C_{org}$ values range from −2.59‰ to −1.96‰, −10.7‰ to −9.0‰, and −32.2‰ to −26.7‰, respectively (Figs. 6 and 7).

Dolomitic rocks from the Xiaowaitoushan Member have ~3.5 wt% P_2O_5, 13–22 wt% MgO, 0.7–3.7 wt% Al_2O_3, and 0.1–1.3 wt% TOC. Their SiO_2 contents decrease from the bottom upward, with the lowest value being 4.3 wt%. They have variable concentrations of Ba (10–139 ppm), Sr (33–241 ppm), U (0.45–7.8 ppm), V (5.8–63 ppm), Cr (8.1–37 ppm), Pb (2.5–100 ppm), Zn (4.5–48 ppm), and Zr (1.0–63 ppm; Figs. 6 and 7). The $\delta^{13}C_{carb}$, $\delta^{18}O_{carb}$, and $\delta^{13}C_{org}$ values range from −2.58‰ to −2.01‰, −9.1‰ to −8.2‰, and −30.7‰ to −23.7‰, respectively (Fig. 7). Phosphorite nodules have the highest Sr (604 ppm) and Ba (139 ppm)

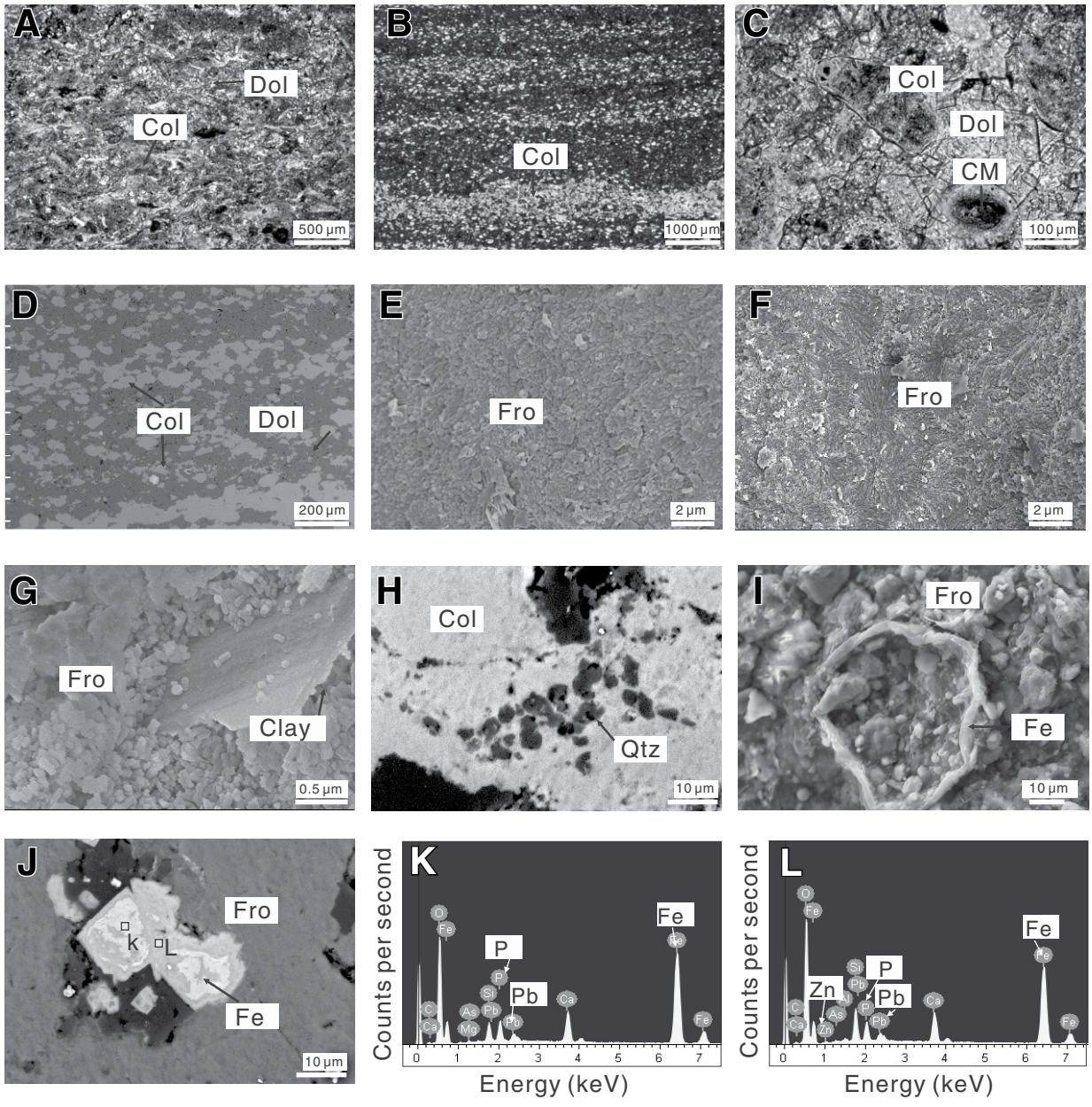

Figure 5. (A–C) Optical images; (D, H, J) backscattered electron (BSE) images; (E, F, G, and I) secondary electron images (SEIs); and (K,L) energy dispersive spectroscopy (EDS) spectra of the upper unit of phosphorite in Meishucun: (A) laminated phosphorite, (B, D) massive phosphorite and sand-sized granules, (C) carbonaceous matter and oolitic grains, (E) stumpy francolites, (F) radial aggregated francolites, (G) francolites around clay mineral, (H) authigenic quartz in a phosphorite granule, (I) iron crust, (J) Fe-oxides, and (K–L) composition of iron parts. CM—carbonaceous matter, Col—collophanite, Dol—dolomite, Fe—Fe-oxides, Fro—francolite, P—phosphorus, Pb—lead, Qtz—quartz, Zn—zinc.

concentrations and the lowest $\delta^{13}C_{carb}$ (–3.32‰), $\delta^{18}O_{carb}$ (–9.3‰), and $\delta^{13}C_{org}$ (–33.7‰) values.

Dolomitic rocks from the Dahai Member contain <7 wt% P_2O_5, 13–20 wt% MgO, 0.3–1.8 wt% Al_2O_3, and ~0.1 wt% TOC. They show high concentrations of Pb (19–33 ppm) and Zn (134–141 ppm). Their $\delta^{13}C_{carb}$, $\delta^{18}O_{carb}$, and $\delta^{13}C_{org}$ values range from –0.31‰ to +0.63‰, –8.4‰ to –7.0‰, and –32.5‰ to –30.1‰, respectively (Fig. 7).

Phosphorites

Phosphorites of the Zhongyicun Member have 14–38 wt% P_2O_5, 0.09–0.66 wt% Na_2O, <13.7 wt% MgO, <10 wt% Al_2O_3, 75–331 ppm Ba, and 247–895 ppm Sr. The cherty layer at the uppermost part of the lower unit is made up of 66 wt% SiO_2 and 12.4 wt% P_2O_5. Phosphorites from the upper unit contain higher Fe_2O_3 (0.2–0.7 wt%), MnO (0–0.1 wt%), TOC (0.1–0.7 wt%), V (18–55 ppm), Cr (20–62 ppm), Pb (15–845 ppm), Cd (0.1–0.7 ppm), and Zn (40–186 ppm) and lower Mo (0.3–1.0 ppm), U (5–18 ppm),

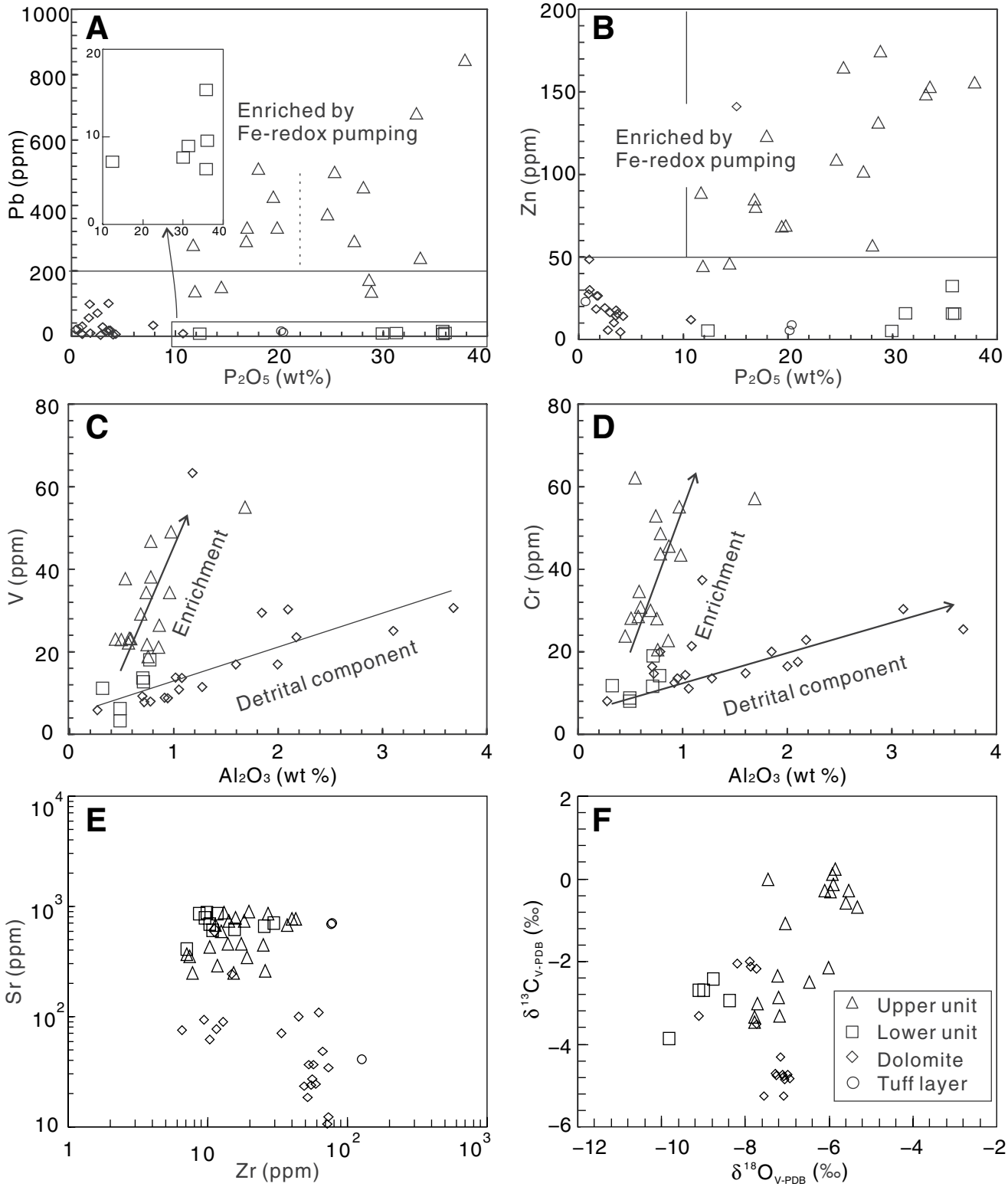

Figure 6. $\delta^{13}C_{carb}$ and $\delta^{18}O_{carb}$ correlation and multi-element diagrams comparing the composition of the dolostones from the Baiyanshao and Xiaowaitoushan Members and phosphorites from the lower and upper units and tuff layer of the Zhongyicun Member of the Zhujiaqing Formation. V-PDB—Vienna Peedee belemnite.

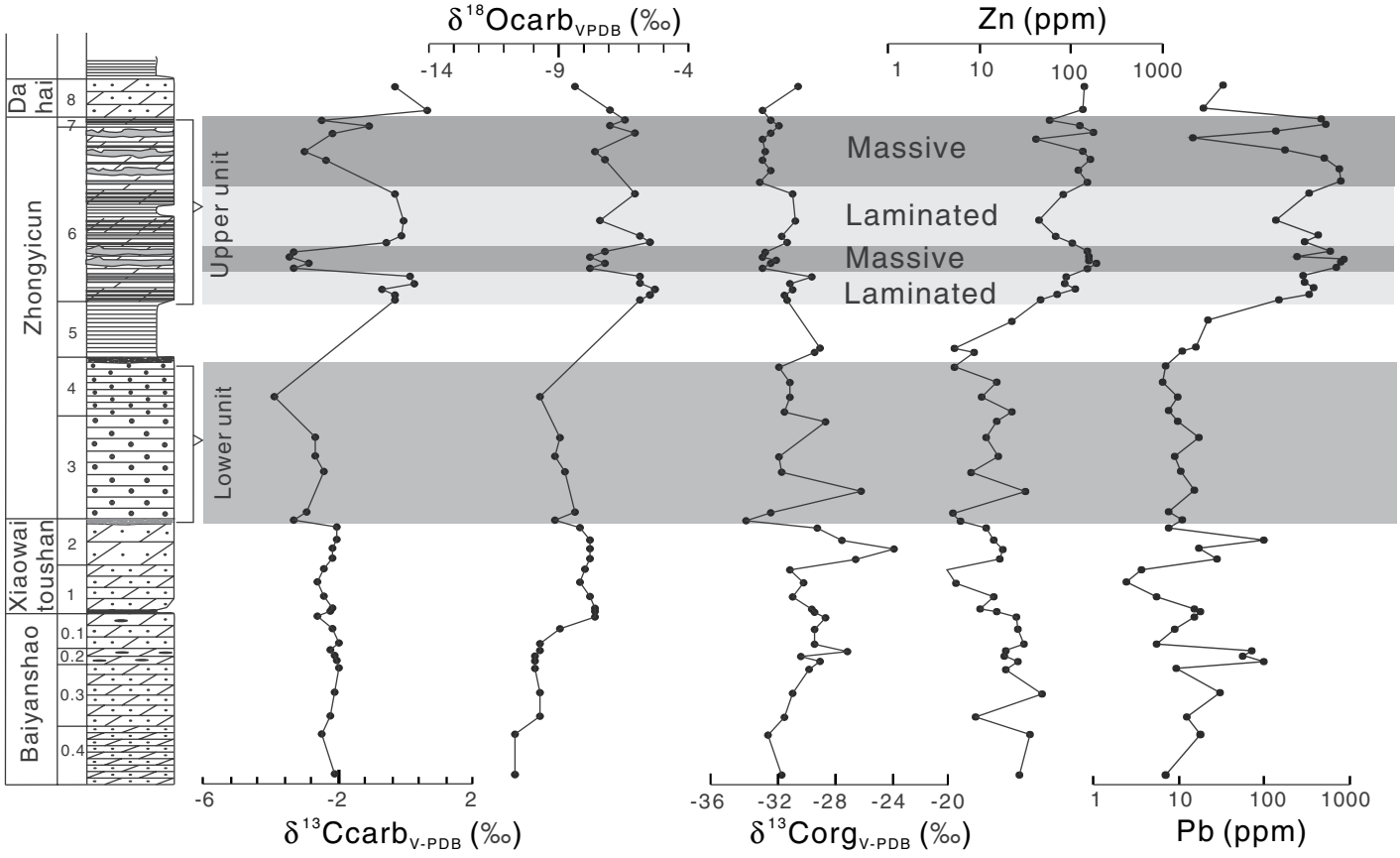

Figure 7. Chemostratigraphic columns of elemental and isotopic compositions, $\delta^{13}C_{carb}$, $\delta^{18}O_{carb}$, $\delta^{13}C_{org}$, Zn, and Pb in the Meishucun section, SW China. VPDB—Vienna Peedee belemnite. For legend and units for stratigraphic column, see Figure 2.

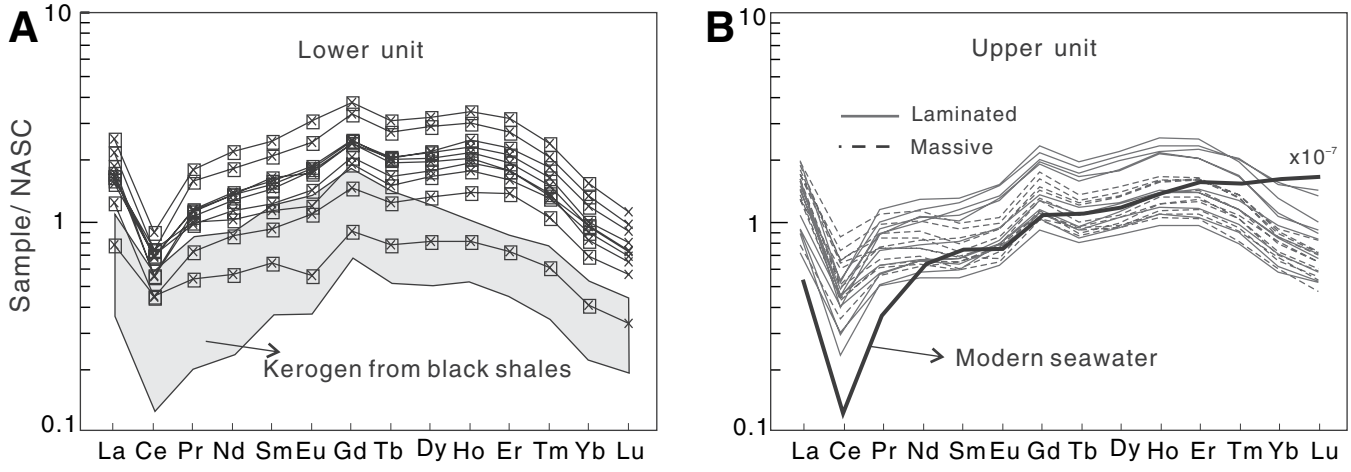

Figure 8. Rare earth element (REE) distribution patterns of phosphorite in the lower and upper units normalized to North American shale composite (NASC). Data for organic matter in the early Cambrian black shale are cited from Pi et al. (2013); modern seawater REE patterns are defined by a water sample at 900 m depth in the North Atlantic (Elderfield and Greaves, 1982).

and middle (M) REE contents (12–31 ppm) than the lower unit (Figs. 6–8; supplementary Table C1 [see footnote 1]). Carbonates of the lower unit have lower $\delta^{13}C_{carb}$ (–3.87‰ to –2.43‰) and $\delta^{18}O_{carb}$ (–9.8‰ to –8.4‰) values than the upper unit, with $\delta^{13}C_{carb}$ (–3.33‰ to +0.24‰) and $\delta^{18}O_{carb}$ (–7.8‰ to –5.3‰). The $\delta^{13}C_{org}$ values of the lower unit range from –32.0‰ to –25.9‰, whereas the upper unit has a narrow range of $\delta^{13}C_{org}$ values from –32.7‰ to –29.1‰ (Fig. 7). Laminated phosphorites in the upper unit have higher δCe and lower δEu values than massive phosphorites (Fig. 8B).

DISCUSSION

Contrasting Processes of Phosphogenesis

Marine phosphorites occur in a variety of forms, such as amorphous, oolitic, and pebble-like textures, and laminated and massive structures (Follmi, 1996). Numerous models have been proposed to explain the phosphogenesis, including abiogenic or organic media accretion (e.g., Swett and Crowder, 1982; She et al., 2013), replacement of biogenic grains (e.g., Salama et al., 2015), and reworking of previous phosphate deposits (e.g., Pufahl and Grimm, 2003; Soudry et al., 2013), where each kind of phosphorite was thought to have formed under a particular environment. Given that phosphorites from the lower and upper units in Meishucun have distinct lithofacies, mineralogy, and geochemical signatures, it is likely that they formed through different pathways.

P Enrichment in Pore Waters

Fluviatile flux and ocean upwelling are major mechanisms that bring phosphorus to shallow seawater on the shelf (Cook and Shergold, 1986). However, neither of these processes is able to provide sufficient phosphorus to generate P-saturated water columns, even under intense continental weathering or oceanic circulation conditions (Follmi, 1996). Francolite is thought to be most likely precipitated beneath the seafloor during diagenesis, within 15–20 cm of the sediment-water interface. Accordingly, both organisms and Fe-(oxyhydr)oxides can effectively enrich P in the pore water by stepwise processes of uptaking/adsorbing phosphate in the shallow water, sinking onto the seafloor, and releasing the phosphate after burial (Follmi, 1996; Nelson et al., 2010; Papineau et al., 2013).

Biological regeneration in the lower unit. Phosphorus is an essential component of life. Breaking down of organic-bounded phosphates would release phosphorus to the interstitial water in sediments during diagenesis (Follmi, 1996). In phosphorites granules and cement from the lower unit in Meishucun, carbonaceous matter and colonies of microfossils are common (Fig. 3), implying that phosphorus in the lower unit was concentrated by the decay of abundant preexisting organisms. Recent studies have argued that giant sulfur bacteria living in coastal water had the potential to generate and release phosphates into anoxic sediments and promote phosphogenesis (Bailey et al., 2007; Schulz and Schulz, 2005). However, giant sulfur bacteria commonly have cell diameters between 100 and 400 μm (Bailey et al., 2007), which are inconsistent with the size of most of the microfossils preserved in phosphorites (4–15 μm; Fig. 3E).

Phosphorites from the lower unit have higher $(Sm/Nd)_N$ and lower $(Ho/Gd)_N$ than rocks from the upper unit and from modern seawater (Elderfield and Greaves, 1982), but similar values to that of kerogen extracted from early Cambrian black shales (Fig. 8A; Pi et al., 2013). They also have lower $\delta^{13}C_{carb}$ values than the underlying dolostones from the Xiaowaitoushan Member and the overlying laminated phosphorites from the upper unit of the Zhongyicun Member. Because decomposed organic matter is a possible source of REEs and ^{12}C for dolomitic phosphorite (Felitsyn and Morad, 2002; Jiang et al., 2012), the negative shifts of $\delta^{13}C_{carb}$ and kerogen-like REE patterns of the lower unit support the assumption that the biological regeneration led to P enrichment in the bottom water. Although negative $\delta^{13}C_{carb}$ excursions are also thought to be led by the upwelling of deep water that is rich in dissolved organic carbon (cf. Banerjee et al., 1997), the $\delta^{13}C_{carb}$ and $\delta^{18}O_{carb}$ covariance and decoupled C isotopes of carbonate and organic matter from rocks of the lower unit argue for a diagenetic origin (Fig. 7; Jiang et al., 2012). Moreover, extensive upwelling usually results in Cd enrichment (Nathan et al., 1997), inconsistent with the Cd depletion (<0.7 ppm) of the lower unit in Meishucun.

Organic matter extracted from the lower unit has a large range of $\delta^{13}C_{org}$ values (–32.0‰ to –25.9‰; Fig. 7). Because diagenesis and metamorphism have minimal effects on $\delta^{13}C_{org}$, Papineau et al. (2013) proposed that such a large range of $\delta^{13}C_{org}$ values cannot be solely due to a postdepositional process, but it is probably due to the combined influence of both buried photoautotrophic biomass and chemoautotrophic organisms in sediments. During carbon fixation, regenerated carbon has been shown to become incorporated in chemoautotrophic organisms, and the chemoautotrophic biomass can be up to 15‰ more depleted in $\delta^{13}C$ relative to the primary photosynthate (Jiang et al., 2012). In addition, pyrite grains in authigenic quartz (Figs. 3G and 3J) suggest that the organic matter was partially oxidized by sulfates during diagenesis (Bottrell and Newton, 2006).

Fe-redox pumping in the upper unit. In contrast, collophanite in the upper unit does not contain abundant organic relics and fossils (Fig. 5). Rocks from this unit have seawater-like REE patterns with higher HREEs than the lower unit and kerogen extracted from early Cambrian black shales (Fig. 8B), indicating only a small contribution from organisms during the formation of the upper unit. Covariations of $\delta^{13}C_{carb}$ and $\delta^{13}C_{org}$ in the upper unit further imply that organic carbon was mainly derived from primary (photosynthetic) production without substantial secondary alteration (e.g., organic remineralization; Fig. 7; cf. Jiang et al., 2012).

As demonstrated by studies of P accumulation in modern coastal areas where there is no mass accumulation of organic matter, insoluble Fe-(oxyhydr)oxide particles can act as an alternative medium for P accumulation by providing adsorption sites for phosphates, which helps to transfer the phosphates into sediments (Heggie et al., 1990). After burial, the adsorbed phosphates can be liberated to pore waters via the dissolution of Fe-(oxyhydr)oxides below the Fe-redox boundary in sediments. As the ferrous ions tend to be re-oxidized above the Fe-redox boundary, the cycling of Fe, known as Fe-redox pumping, can cause phosphorus to be effectively removed from the seawater and subsequently enriched in the pore water (Follmi, 1996; Nelson et al., 2010). In the upper unit of the Meishucun section, Fe-oxides contain large amounts of phosphorus (Figs. 5J–5L), implying that their phosphorus enrichment might have been regulated by Fe-redox pumping.

Rocks from the upper unit have 15–845 ppm Pb and 41–185 ppm Zn, i.e., more than eight times higher than rocks from the lower unit (Pb = 6–17 ppm and Zn = 5–32 ppm). Heavy metals would not have been extracted from the underlying tuff layer, because the tuff layers have very low Pb (11–23 ppm) and Zn (5–23 ppm) concentrations relative to the upper unit (Fig. 7). Lead and Zn concentrations of the phosphorites show no linear correlation with Al_2O_3 and TOC (supplementary Fig. A3 [see footnote 1]) but are positively correlated with P_2O_5 (Figs. 6A and 6B), indicating that they are mainly preserved in authigenic phosphate-bearing minerals rather than in detrital components or organic matter. It has been suggested that redox-insensitive Pb and Zn from a water column tend to be adsorbed by Fe-(oxyhydr)oxides (Li et al., 2001). After being released through decomposition of Fe-(oxyhydr)oxides, both Pb and Zn can readily be taken up by CO_3^{2-} or PO_4^{3-} and precipitated in sediments (Cao et al., 2004; Mann and Deutscher, 1980) or adsorbed by francolite

(Prasad et al., 2002). In this regard, the high Pb and Zn concentrations in rocks from the upper unit support our interpretation that P enrichment in bottom waters during the formation of the upper unit was regulated by Fe-(oxyhydr)oxide adsorption and subsequent desorption after burial.

Precipitation

Precipitation of francolite occurs mainly through (1) replacement of biodetritus (e.g., Manheim et al., 1980), (2) adsorption by biogenetic/abiogenetic nuclei (e.g., She et al., 2013), or (3) direct crystallization in water columns supersaturated with calcium phosphate (e.g., Nelson et al., 2010). The small crystal size of francolite from Meishucun phosphorites combined with the lack of biodetritus textures argue against the replacement process (Figs. 4 and 5).

Adsorption on organism substrates. Abundant radial and tufted aggregates of francolite are present in granules and cements of rocks from the lower unit (Figs. 4B–4E). In order to form the radial or tufted shape, multinuclei substrates would be required in the inner part of the aggregates for phosphate precipitation. Among all common particles of phosphorites from the lower unit, including organic matter, carbonates, quartz, and clay minerals, organic matter has the most abundant anionic carboxyl and hydroxyl groups that can chelate seed particles that act as the nuclei (She et al., 2013). Radial and tufted apatite aggregates grown on organic multinuclei substrates (hexadecyltrimethylammonium bromide) have already been synthesized in the laboratory (Yang et al., 2013). Based on the observation that radial and tufted textures in rocks from the lower unit are preferentially and systematically associated with carbonaceous matter (Figs. 4A–4C), we interpret that the francolite in the lower unit crystallized dominantly by adsorption on organism substrates. In addition, relatively small francolite grains inside or near microfossils are consistent with rapid precipitation on numerous nucleation sites, and a reduction in the space for the growth of larger apatite crystals (Figs. 4B and 4C). Once formed, francolite grains would serve as new templates for further francolite accretion (Follmi, 1996), and thus later-formed francolite grains are orientated toward the organic nuclei (Figs. 4B–4E). Francolite grains that precipitated in an area with trace amounts of carbonaceous matter are larger in size (>1 μm) due to the available space for growth (Figs. 4D and 4E). The texture and precipitation mode of francolite in the lower unit are analogous to in situ microbially mediated accretionary growth, and the best multinuclei are considered as extracellular polymeric substances produced by cyanobacteria (She et al., 2013).

P supersaturation in Si-rich pore waters. In the upper unit, only small proportions of francolite grains grow on the surface of clay minerals or organic nuclei, whereas the majority are stumpy and randomly orientated (Fig. 5E). Authigenic quartz that grows within collophanite is common in this unit, indicative of Si-saturated bottom waters (Fig. 5H). High-Si contents can significantly reduce P resorption by Fe-(oxyhydr)oxides in bottom waters (Konhauser et al., 2007; Planavsky et al., 2010) and lead to the supersaturation of phosphorus (i.e., >~200 m*M*; Vancappellen and Berner, 1991) and rapid precipitation, even without a well-developed nuclei. Thus, the intergrowth of francolite and authigenic quartz in rocks from the upper unit (Fig. 5H) clearly shows that P precipitation occurred in Si-rich pore waters.

Reworking Process

After deposition, phosphorite can be buried by subsequent sediments as a pristine phase or reworked by high-energy water to become a condensed phosphorite accumulation that has high economic value (Follmi, 1996).

High-energy shallow water. Oolitic textures with concentric thin layers of phosphate granules from the lower unit (Figs. 3B and 3D) clearly reflect a high-energy reworking process when regressed into the high-energy water column (Simone, 1980). The organic-rich phosphoritic intraclasts suspended or rolled on the seafloor and became oolitic in the high-energy water, whereas heavy clasts, including large terrigenous clasts and small shelly fossils, tended to be deposited without additional growth in the P-rich bottom water (Figs. 3C, 3D, and 3J), resulting in microscale stratified structures with phosphorus-rich and clast-rich layers (supplementary Fig. A4 [see footnote 1]). Perhaps to a small extent, phosphorites from other locations were also involved in the sediments. Abundant carbonaceous matter in cement or granular crust (Fig. 3K) indicates that microbially mediated accretion of francolite was also active during or immediately after the reworking process.

Oscillation sea-level changes. In the upper unit, amorphous collophanite in the cement of the laminated phosphorite indicates the possible absence of reworking during a higher sea-level stand (Fig. 5A; Follmi, 1996; Soudry et al., 2013), whereas arenaceous textures of massive phosphorites and ripple marks between laminated and massive phosphorite layers indicate a period of high-energy water above the wave base (supplementary Fig. A5 [see footnote 1]; cf. Ilyin, 1998). Interlayering of laminated and massive phosphorites suggests the ocean was experiencing rapid transgressive-regressive cycles. Uranium substitutes Ca in francolite, but it is generally rare in carbonates and detrital components (cf. Soudry et al., 2002). A positive linear correlation between U and P_2O_5 in the upper unit indicates that the physical reworking process also led to the enrichment of specific elements in phosphates (supplementary Fig. A3 [see footnote 1]). In addition, reworked phosphorite layers have lower $\delta^{13}C_{carb}$ values than the laminated layers (Fig. 7), because the reworked granular phosphorites/carbonates have high porosity and are thus more susceptible to the remineralization of organic matter during diagenesis.

Environmental Reconstruction

Both the upper and lower units have similar Al, Sr, Ba, and Zr concentrations (Fig. 6) and high $^{87}Sr/^{86}Sr$ isotopic ratios (>0.7090; Shields and Stille, 2001), indicative of constant continental weathering rates during phosphogenesis in the early Cambrian. The microbially mediated accretionary growth of phosphorites always takes place when the ocean is oxygenated and during high primary production, e.g., in modern upwelling zones (Burnett et al., 1983), whereas the Fe-redox pumping process relies on a Fe-redox boundary in sediments to allow the transformation between Fe^{3+} and Fe^{2+} (Nelson et al., 2010). We thus propose that the different genetic mechanisms for the lower and upper units in Meishucun may be attributed to an environmental change during the early Cambrian.

Deposition of the Lower Unit under an Oxygenated Water Column

Coccoidal microfossils in the lower unit are generally 4–15 μm in diameter, falling well within the size range of typical cyanobacteria (Figs. 3D and 3E; She et al., 2013). They aggregated and formed dense clusters, showing textures similar to colonies of cyanobacteria fossils in Ediacaran phosphorites of South China (She et al., 2013, 2014). The $\delta^{13}C_{org}$ values (−32.0‰ to −25.9‰) of organic matter are also consistent with that of the cyanobacteria biomass (Eigenbrode and Freeman, 2006). The early Cambrian was also a period of cyanobacterial diversity, which is represented by the widespread occurrence of calcified cyanobacteria (Maloof et al., 2010; Riding, 2006). In the Yangtze block, South China, abundant cyanobacterial fossils have already been discovered in the lower part of the early Cambrian Yanjiahe Formation (equivalent to the Zhujiaqing Formation; Dong et al., 2009). In this regard, formation of the lower unit in Meishucun was closely related to the early Cambrian cyanobacterial proliferation. The increased cyanobacterial population promoted intensive photosynthesis and subsequently

elevated the O_2 concentration in the atmosphere and shallow seawater in the ancient geological period (Papineau et al., 2013).

V and Cr concentrations of phosphorites from the lower unit and dolostones of the Baiyanshao and Xiaowaitoushan Members show positive linear correlations with Al_2O_3 (Figs. 6C and 6D), indicating that they were mainly incorporated in detritus. Because both redox-sensitive elements V and Cr have high solubilities in their high valence forms of VO_3^-/VO_4^{3-} and CrO_4^{2-} (Tribovillard et al., 2006), low concentrations of V and Cr also imply deposition of the lower unit under a relatively oxic environment without excess V and Cr enrichment. Mo isotopes are widely used to determine the depositional environments for marine sediments (Chen et al., 2015; Goldberg et al., 2009). As reported by Wen et al. (2011), phosphorites from the lower unit have low $\delta^{97/95}$Mo values, ranging from –0.15‰ to –0.53‰, relative to those from the upper unit, with $\delta^{97/95}$Mo values of +0.89‰ to +1.40‰. Those authors proposed that the low $\delta^{97/95}$Mo values in the lower unit were the result of deposition of Fe-(oxyhydr)oxides during a reworking process, reflecting secondary modification in an oxic water column. However, the oolitic granules are cemented in a phosphatic matrix (Figs. 3 and 4), clearly indicating that phosphogenesis was still active during the development of the oolitic textures. Thus, we propose that the low $\delta^{97/95}$Mo values reflect the deposition and reworking processes of the lower unit in oxic seawater with abundant Fe-(oxyhydr)oxides that could adsorb the light Mo isotope and sink to the water-sediment interface.

In contrast, the presence of pyrite in authigenic quartz from rocks of the lower unit implies a pronounced redox gradient from oxic to anoxic conditions across the water-sediment interface (Fig. 4). In sediments where abundant microbial biomass has accumulated, such a pronounced redox gradient is usually attributed to immediate O_2 consumption by the decay of organisms beneath the water-sediment interface (Kristensen, 2000; Tay et al., 2013). During diagenesis, some of the Fe-(oxyhydr)oxides were decomposed by humic acids and reduced in an anoxic environment. Mo adsorbed on Fe-(oxyhydr)oxides was released and converted from MoO_4^{2-} to insoluble $MoO_xS_{4-x}^{2-}$ after reacting with the reduced hydrogen sulfide (Goldberg et al., 2009), resulting in the light $\delta^{97/95}$Mo isotopic signature in the lower unit.

Deposition of the Upper Unit near the Fe-Redox Boundary

Rocks from the upper unit have higher V and Cr concentrations and fewer cyanobacteria fossils than the lower unit (Figs. 5 and 6). V and Cr would be reduced from their soluble forms to the readily adsorbed VO_2^+ ion and $Cr(OH)_3$. Thus, enrichment of V and Cr reflects oxygen deficiency during the formation of the upper unit (Figs. 6C and 6D; Pi et al., 2013). As phosphorus accumulation in the upper unit was regulated by Fe-pumping, bottom waters within the Fe-oxide zone would have been required to prevent the decomposition of Fe-(oxyhydr)oxides before reaching the seafloor. On the other hand, to release phosphorus to pore waters, the redox state just beneath the water-sediment interface was interpreted to be below the Fe-redox boundary (Nelson et al., 2010). High $\delta^{97/95}$Mo values and low Mo concentrations in the upper unit suggest that MoO_4^{2-} released from decomposition of Fe-(oxyhydr)oxides was rarely converted to $MoO_xS_{4-x}^{2-}$, which is readily deposited in sediments. Thus, the upper unit was deposited near the Fe-redox boundary and above the sulfur reduction zone, and Mo with high a $\delta^{97/95}$Mo signature was mostly incorporated from the seawater (Wen et al., 2011). The relatively reducing environment diminished the contamination of Mo isotopes from surviving Fe oxides in sediments. This is why Fe oxides that precipitate under an oxygen-deficient water column (e.g., magnetite and ferrihydrite) have $\delta^{97/95}$Mo values much closer to the ambient water than their counterparts that form under oxic conditions (e.g., goethite and hematite; supplementary Fig. A6 [see footnote 1]; Goldberg et al., 2009).

Oceanic Reduction Caused by ca. 535 Ma Volcanism and Hydrothermal Venting

As discussed already, the redox states of the early Cambrian seawaters recorded in Meishucun phosphorites changed from oxic to anoxic near the Fe-redox boundary. This change cannot solely be attributed to oceanic transgression at the depositional site of the Meishucun phosphorites from a high-energy water zone down to (or near) the wave base, because a transgression is not able to explain the simultaneously decreasing bioproductivity in the ocean. The presence of abundant small shelly fossils below the tuff layer (Figs. 3C and 3F) indicates that the biologically unfavorable environment may have been caused by a ca. 535 Ma volcanic event. In fact, volcanic layers are widely distributed in the southeastern margin of the Yangtze block and include the ca. 532.3 Ma tuff layer in the lower Niutitang Formation at Songlin, Guizhou Province (Jiang et al., 2009), the ca. 536 Ma tuff layer in the upper Laobao Formation at Pingyin, Guizhou Province (Zhou et al., 2013), and the ca. 536.3 Ma tuff layer above the Liuchapo Formation at Ganziping, Hunan Province (Chen et al., 2009). In addition, cherty layers in the middle part of the Zhongyicun Member in Laolin, Yunnan Province, and in the Liuchapo Formation in Ganziping, Hunan Province (Chen et al., 2009; Li et al., 2009), suggest that volcanism-related submarine hydrothermal venting was widespread in the ocean basin (Chen et al., 2009). Abundant authigenic quartz and negative δ^{30}Si isotopic values (–0.4‰; Y.H. Li et al., 1995; Fan et al., 2013) in the upper unit confirm the involvement of hydrothermal fluids during their deposition. In addition, the upper Zhujiaqing Formation in the Laolin area shows a negative shift of $\delta^{13}C_{carb}$ values (Li et al., 2009), which may be indicative of a release of CH_4 into the ocean accompanying the hydrothermal venting. The reducing hydrothermal fluids with abundant H_2S and CH_4 might have resulted in climate warming, oceanic oxygen deficiency, oceanic poisoning, and subsequent mass extinction (Charlou et al., 2002; Chen et al., 2009). Thus, a causal link between the ca. 535 Ma volcanism and environmental change can be inferred.

Genetic Model and its Implications

A two-stage conceptual model for the generation of phosphorites in Meishucun can be constructed (Fig. 9). The lower unit was formed in an oxic and highly productive ocean where organisms, particularly cyanobacteria, extracted phosphorus from seawaters. After burial, anaerobic oxidation of organisms released PO_4^{3-} and ^{13}C-depleted HCO_3^- back to the bottom water to form francolite and ^{13}C-depleted carbonates. Although most H_2S generated at this time was reoxidized, some portion was captured by Fe^{2+} and formed pyrite during diagenesis. Organisms also provided the nuclei for francolite precipitation. The lower unit is interpreted to have been reworked in a high-energy water column (Fig. 9A), resulting in the oolitic texture and massive structure of phosphorites (supplementary Fig. A4 [see footnote 1]). Marine volcanism and hydrothermal venting at ca. 535 Ma led to oxygen reduction and a decrease of bioproductivity in the marine environment. The upper unit may have formed in the shallow ocean with low productivity, where organisms were not the dominant source of phosphorus. The phosphorus enrichment in this unit was promoted by Fe-redox pumping. The recycling of iron also led to the incorporation of Zn and Pb in phosphorites (Fig. 9B). Ripple marks along the boundary of laminated and massive phosphorite layers clearly show regression-related reworking (supplementary Fig. A5 [see footnote 1]). Primary collophanite was concentrated near the sediment-water interface under high-energy conditions. Light dolomite fragments were washed out, whereas heavy collophanite grains were compacted (supplementary Fig. A5 [see footnote 1]).

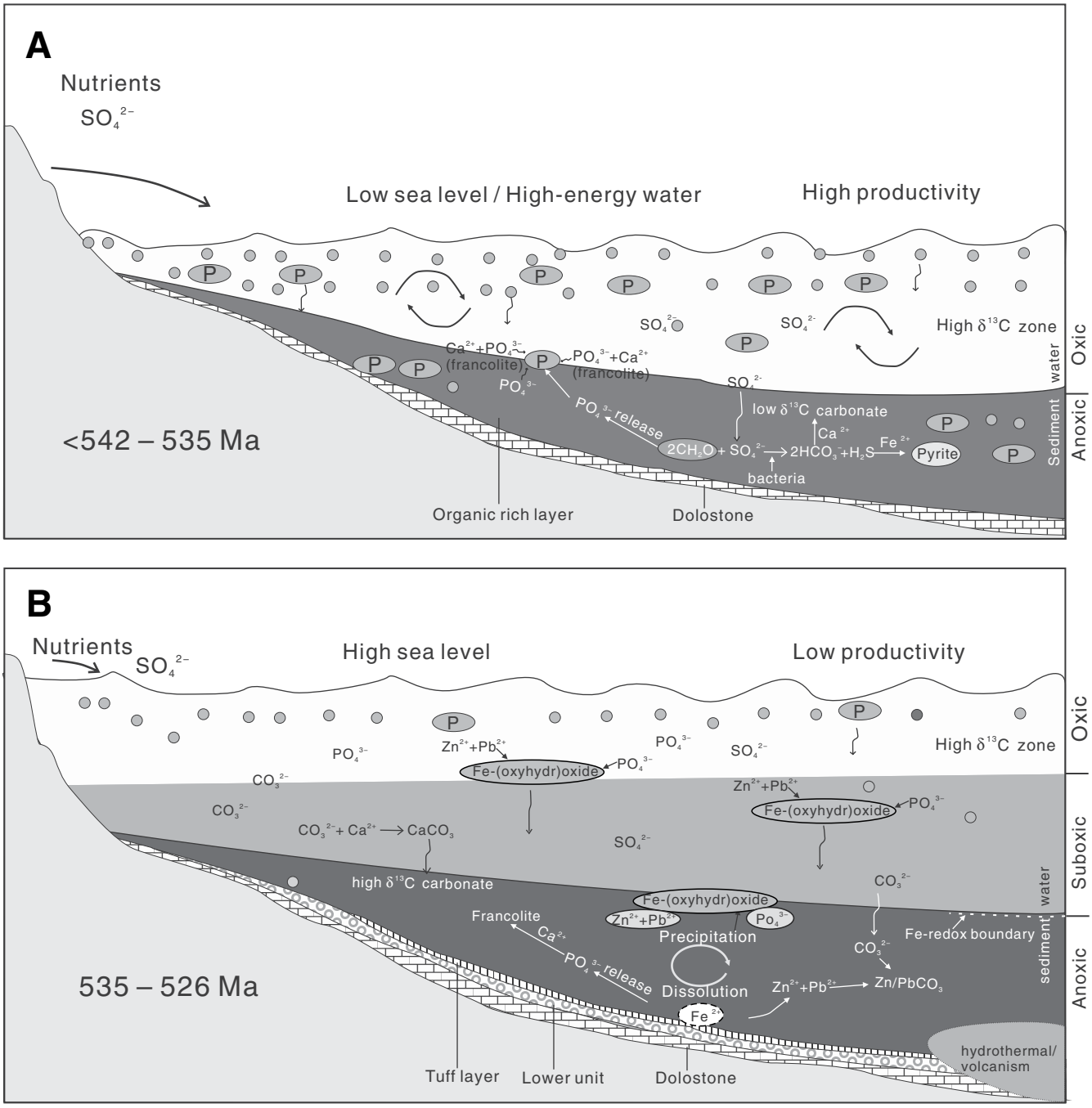

Figure 9. Schematic conceptual model illustrating different phosphogenesis mechanisms in the lower and upper units of phosphorite in Meishucun and environmental change at the early Cambrian. (A) Lower unit formed within high-productivity oxygenated seawater, where the P-enrichment process includes P adsorption by organisms from oxic seawater and P regeneration after decomposition of organic matter in anoxic sediments. (B) Upper unit deposited under a suboxic water column, where Fe-redox pumping led to accumulation of P, Zn, and Pb in the sediments.

Postdepositional reworking led to rapid oxidation of previously accumulated organisms and low $\delta^{13}C_{carb}$ values of carbonates. Alternating pristine and reworked phosphorites suggest that the upper unit was formed under conditions of rapid sea-level change (Ilyin, 1998).

Ediacaran–Cambrian marine sediments worldwide have high $^{87}Sr/^{86}Sr$ values (>0.7090), showing that Earth experienced extensive weathering due to the breakup of Rodinia and assembly of Gondwanaland (Halverson et al., 2009; Montanez and Soreghan, 2006). During this time period, the increased phosphate availability from continental input likely caused cyanobacterial proliferation and played a key role in the oxygenation of Earth's atmosphere (Papineau et al., 2013). Most early Cambrian phosphorites in the world are depleted in

HREEs (Ilyin, 1998; Shields and Stille, 2001), and they have $(Sm/Nd)_N > 1$ and $(Ho/Gd)_N < 1$, similar to the REE patterns of the lower unit in Meishucun (supplementary Fig. A7 [see footnote 1]). These similarities indicate a significant contribution of organic regeneration to the global phosphogenesis.

It is unclear if the subsequent decrease of oxygen concentration and bioproductivity in the shallow water, as recorded in the upper unit in Meishucun, existed worldwide or was simply restricted to the Yangtze block, South China, due to the lack of robust lithostratigraphic and geochronologic correlations between basins. However, there is general agreement that there was a diverse worldwide fossil assemblage during 534–530 Ma that was associated with rapid reorganizations of the carbon cycle, long-term rising of sea level, and hydrothermal fluxes of Sr (Maloof et al., 2010). Assuming that the shallow water column above the wave base was well mixed and was in equilibrium with atmospheric oxygen, subsequent decreases of oxygen recorded in the upper unit may have been a global phenomenon. The redox states of the early Cambrian ocean have been a matter of debate for the past decades, and most lines of evidence have come from deep-ocean sediments (Chen et al., 2015; Jiang et al., 2006, 2009; Wille et al., 2008). The present study suggests that the shallow ocean may also have experienced redox changes at the dawn of life in the early Cambrian.

CONCLUSIONS

Phosphorites in the lower unit of the Zhongyicun Member of the Zhujiaqing Formation in Meishucun formed by means of biological utilization and adsorption of P, whereas those in the upper unit were generated through Fe-redox pumping and precipitation in P-saturated pore water. The lower unit was physically further concentrated under a high-energy water column, whereas bedded phosphorites in the upper unit formed during oscillating sea-level changes. Differing phosphogenesis mechanisms in the lower and upper units may have been related to oxygen consumption caused by submarine volcanism that released large amounts of CH_4 and H_2S to the bottom water. Cyanobacterial proliferation in the early Cambrian contributed to the global phosphogenesis. The subsequent oxygen deficiency in the ocean recorded in the upper unit suggests that the redox state in the shallow ocean was oscillatory during the early Cambrian.

ACKNOWLEDGMENTS

This research was financially supported by the Research Grant Council of Hong Kong (17306814), the Committee on Research and Conference Grants of the University of Hong Kong, and research grant of State Key Laboratory for mineral Deposits Research (2014-03). We thank Xinfu Zhao for his assistance in the field and Liang Qi for the trace-element analysis. We thank Wei Wang and Zhou Wang for reading an early draft of this paper and for their insightful comments. The constructive and detailed comments from the editor (Aaron J. Cavosie), associate editor (Gregory K. Druschel), and three journal reviewers (Chris Reinhard and two anonymous reviewers) are highly appreciated.

REFERENCES CITED

Anbar, A.D., and Knoll, A.H., 2002, Proterozoic ocean chemistry and evolution: A bioinorganic bridge?: Science, v. 297, no. 5584, p. 1137–1142, doi:10.1126/science.1069651.

Bailey, J.V., Joye, S.B., Kalanetra, K.M., Flood, B.E., and Corsetti, F.A., 2007, Evidence of giant sulphur bacteria in Neoproterozoic phosphorites: Nature, v. 445, no. 7124, p. 198–201, doi:10.1038/nature05457.

Banerjee, D.M., Schidlowski, M., Siebert, F., and Brasier, M.D., 1997, Geochemical changes across the Proterozoic-Cambrian transition in the Durmala phosphorite mine section, Mussoorie hills, Garhwal Himalaya, India: Palaeogeography, Palaeoclimatology, Palaeoecology, v. 132, no. 1-4, p. 183–194, doi:10.1016/S0031-0182(97)00060-6.

Bottrell, S.H., and Newton, R.J., 2006, Reconstruction of changes in global sulfur cycling from marine sulfate isotopes: Earth-Science Reviews, v. 75, no. 1-4, p. 59–83, doi:10.1016/j.earscirev.2005.10.004.

Burnett, W.C., Roe, K.K., and Piper, D.Z., 1983, Upwelling and phosphorite formation in the ocean, *in* Suess, E., Thiede, E., and Thiede, J., eds., Coastal Upwelling: Its Sediment Record: New York, Plenum Press, p. 377–397.

Cao, X.D., Ma, L.Q., Rhue, D.R., and Appel, C.S., 2004, Mechanisms of lead, copper, and zinc retention by phosphate rock: Environmental Pollution, v. 131, no. 3, p. 435–444, doi:10.1016/j.envpol.2004.03.003.

Charlou, J., Donval, J., Fouquet, Y., Jean-Baptiste, P., and Holm, N., 2002, Geochemistry of high H_2 and CH_4 vent fluids issuing from ultramafic rocks at the Rainbow hydrothermal field (36°14′N, MAR): Chemical Geology, v. 191, no. 4, p. 345–359, doi:10.1016/S0009-2541(02)00134-1.

Chen, D.Z., Wang, J.G., Qing, H.R., Yan, D.T., and Li, R.W., 2009, Hydrothermal venting activities in the early Cambrian, South China: Petrological, geochronological and stable isotopic constraints: Chemical Geology, v. 258, no. 3-4, p. 168–181, doi:10.1016/j.chemgeo.2008.10.016.

Chen, X., Ling, H.F., Vance, D., Shields-Zhou, G.A., Zhu, M.Y., Poulton, S.W., Och, L.M., Jiang, S.Y., Li, D., Cremonese, L., and Archer, C., 2015, Rise to modern levels of ocean oxygenation coincided with the Cambrian radiation of animals: Nature Communications, v. 6, p. 7142, doi:10.1038/ncomms8142.

Compston, W., Zhang, Z., Cooper, J.A., Ma, G.G., and Jenkins, R.J.F., 2008, Further SHRIMP geochronology on the early Cambrian of South China: American Journal of Science, v. 308, no. 4, p. 399–420, doi:10.2475/04.2008.01.

Cook, P.J., and Shergold, J.H., 1986, Phosphate Deposits of the World: Volume 1: Proterozoic and Cambrian Phosphorites: Cambridge, UK, Cambridge University Press, 408 p.

Dong, L., Xiao, S., Shen, B., Zhou, C., Li, G., and Yao, J., 2009, Basal Cambrian microfossils from the Yangtze Gorges area (South China) and the Aksu area (Tarim block, northwestern China): Journal of Paleontology, v. 83, no. 1, p. 30–44, doi:10.1017/S0022336000058108.

Eigenbrode, J.L., and Freeman, K.H., 2006, Late Archean rise of aerobic microbial ecosystems: Proceedings of the National Academy of Sciences of the United States of America, v. 103, no. 43, p. 15,759–15,764, doi:10.1073/pnas.0607540103.

Elderfield, H., and Greaves, M.J., 1982, The rare earth elements in seawater: Nature, v. 296, no. 5854, p. 214–219, doi:10.1038/296214a0.

Fan, H.F., Wen, H.J., Zhu, X.K., Hu, R.Z., and Tian, S.H., 2013, Hydrothermal activity during Ediacaran-Cambrian transition: Silicon isotopic evidence: Precambrian Research, v. 224, p. 23–35, doi:10.1016/j.precamres.2012.09.004.

Felitsyn, S., and Morad, S., 2002, REE patterns in latest Neoproterozoic–early Cambrian phosphate concretions and associated organic matter: Chemical Geology, v. 187, no. 3, p. 257–265, doi:10.1016/S0009-2541(02)00046-3.

Follmi, K.B., 1996, The phosphorus cycle, phosphogenesis and marine phosphate-rich deposits: Earth-Science Reviews, v. 40, no. 1-2, p. 55–124, doi:10.1016/0012-8252(95)00049-6.

Goldberg, T., Archer, C., Vance, D., and Poulton, S.W., 2009, Mo isotope fractionation during adsorption to Fe (oxyhydr) oxides: Geochimica et Cosmochimica Acta, v. 73, no. 21, p. 6502–6516, doi:10.1016/j.gca.2009.08.004.

Guo, Q.J., Shields, G.A., Liu, C.Q., Strauss, H., Zhu, M.Y., Pi, D.H., Goldberg, T., and Yang, X.L., 2007, Trace element chemostratigraphy of two Ediacaran–Cambrian successions in South China: Implications for organosedimentary metal enrichment and silicification in the early Cambrian: Palaeogeography, Palaeoclimatology, Palaeoecology, v. 254, no. 1-2, p. 194–216, doi:10.1016/j.palaeo.2007.03.016.

Halverson, G.P., Hurtgen, M.T., Porter, S.M., and Collins, A.S., 2009, Neoproterozoic–Cambrian biogeochemical evolution, *in* Gaucher, C., Sial A.N., Frimmel, H.E., and Halverson, G.P., eds., Neoproterozoic–Cambrian Tectonics, Global Change and Evolution: A Focus on South Western Gondwana: Oxford, Elsevier, Developments in Precambrian Geology 16, p. 351–365.

Heggie, D., Skyring, G., O'Brien, G., Reimers, C., Herczeg, A., Moriarty, D., Burnett, W., and Milnes, A., 1990, Organic carbon cycling and modern phosphorite formation on the East Australian continental margin: An overview, *in* Notholt, A.J.G., and Jarvis, I., eds., Phosphorite Research and Development: Geological Society, London, Special Publication 52, p. 87–117, doi:10.1144/GSL.SP.1990.052.01.07.

Ilyin, A.V., 1998, Rare-earth geochemistry of 'old' phosphorites and probability of syngenetic precipitation and accumulation of phosphate: Chemical Geology, v. 144, no. 3-4, p. 243–256, doi:10.1016/S0009-2541(97)00134-4.

Ishikawa, T., Ueno, Y., Komiya, T., Sawaki, Y., Han, J., Shu, D.G., Li, Y., Maruyama, S., and Yoshida, N., 2008, Carbon isotope chemostratigraphy of a Precambrian/Cambrian boundary section in the Three Gorge area, South China: Prominent global-scale isotope excursions just before the Cambrian explosion: Gondwana Research, v. 14, no. 1-2, p. 193–208, doi:10.1016/j.gr.2007.10.008.

Jiang, G.Q., Wang, X.Q., Shi, X.Y., Xiao, S.H., Zhang, S.H., and Dong, J., 2012, The origin of decoupled carbonate and organic carbon isotope signatures in the early Cambrian (ca. 542–520 Ma) Yangtze platform: Earth and Planetary Science Letters, v. 317–318, p. 96–110, doi:10.1016/j.epsl.2011.11.018.

Jiang, S.-Y., Chen, Y.-Q., Ling, H.-F., Yang, J.-H., Feng, H.-Z., and Ni, P., 2006, Trace- and rare-earth element geochemistry and Pb-Pb dating of black shales and intercalated Ni-Mo-PGE-Au sulfide ores in Lower Cambrian strata, Yangtze Platform, South China: Mineralium Deposita, v. 41, no. 5, p. 453–467, doi:10.1007/s00126-006-0066-6.

Jiang, S.Y., Pi, D.H., Heubeck, C., Frimmel, H., Liu, Y.P., Deng, H.L., Ling, H.F., and Yang, J.H., 2009, Early Cambrian ocean anoxia in South China: Nature, v. 459, no. 7248, p. E5–E6, doi:10.1038/nature08048.

Kimura, H., and Watanabe, Y., 2001, Oceanic anoxia at the Precambrian-Cambrian boundary: Geology, v. 29, no. 11, p. 995–998, doi:10.1130/0091-7613(2001)029<0995:OAATPC>2.0.CO;2.

Konhauser, K.O., Lalonde, S.V., Amskold, L., and Holland, H.D., 2007, Was there really an Archean phosphate crisis?: Science, v. 315, no. 5816, p. 1234, doi:10.1126/science.1136328.

Kristensen, E., 2000, Organic matter diagenesis at the oxic/anoxic interface in coastal marine sediments, with

emphasis on the role of burrowing animals: Hydrobiologia, v. 426, no. 1, p. 1–24, doi:10.1023/A:1003980226194.

Li, D., Ling, H.F., Jiang, S.Y., Pan, J.Y., Chen, Y.Q., Cai, Y.F., and Feng, H.Z., 2009, New carbon isotope stratigraphy of the Ediacaran-Cambrian boundary interval from SW China: Implications for global correlation: Geological Magazine, v. 146, no. 4, p. 465–484, doi:10.1017/S0016756809006268.

Li, D., Ling, H.F., Shields-Zhou, G.A., Chen, X., Cremonese, L., Och, L., Thirlwall, M., and Manning, C.J., 2013, Carbon and strontium isotope evolution of seawater across the Ediacaran-Cambrian transition: Evidence from the Xiaotan section, NE Yunnan, South China: Precambrian Research, v. 225, p. 128–147, doi:10.1016/j.precamres.2012.01.002.

Li, X.D., Shen, Z.G., Wai, O.W.H., and Li, Y.S., 2001, Chemical forms of Pb, Zn and Cu in the sediment profiles of the Pearl River Estuary: Marine Pollution Bulletin, v. 42, no. 3, p. 215–223, doi:10.1016/S0025-326X(00)00145-4.

Li, Y.H., Wan, D.F., and Jiang, S.Y., 1995, Silicon isotope study on the Meishucun Precambrian-Cambrian boundary section, Yunnan: Geological Review, v. 41, p. 179–187 [in Chinese with English abstract].

Li, Z.-X., Zhang, L., and Powell, C.M., 1995, South China in Rodinia: Part of the missing link between Australia–East Antarctica and Laurentia?: Geology, v. 23, no. 5, p. 407–410, doi:10.1130/0091-7613(1995)023<0407:SCIRPO>2.3.CO;2.

Luo, H.L., Jiang, Z.W., Wu, X.C., Song, X.L., Ouyang, L., Xing, Y.S., Liu, G.Z., Zhang, S.S., and Tao, Y.H., 1984, Sinan-Cambrian Boundary Stratotype section at Meishucun, Jinning, Yunnan, China: Yunnan, China, People's Publishing House, 154 p.

Maloof, A.C., Porter, S.M., Moore, J.L., Dudas, F.O., Bowring, S.A., Higgins, J.A., Fike, D.A., and Eddy, M.P., 2010, The earliest Cambrian record of animals and ocean geochemical change: Geological Society of America Bulletin, v. 122, no. 11-12, p. 1731–1774.

Manheim, F.T., Pratt, R.M., and McFarlin, P.F., 1980, Composition and origin of phosphorite deposits of the Blake Plateau, *in* Bentor, Y.K., ed., Marine Phosphorites—Geochemistry, Occurrence, Genesis: Society of Economic Paleontologists and Mineralogists Special Publication 29, p. 117–137, doi:10.2110/pec.80.29.0117.

Mann, A.W., and Deutscher, R.L., 1980, Solution geochemistry of lead and zinc in water containing carbonate, sulphate and chloride ions: Chemical Geology, v. 29, no. 3-4, p. 293–311, doi:10.1016/0009-2541(80)90026-1.

Montanez, I., and Soreghan, G.S., 2006, Earth's fickle climate: Lessons learned from deep-time ice ages: Geotimes, v. 51, no. 3, p. 24–27.

Nathan, Y., Soudry, D., Levy, Y., Shitrit, D., and Dorfman, E., 1997, Geochemistry of cadmium in the Negev phosphorites: Chemical Geology, v. 142, no. 1-2, p. 87–107, doi:10.1016/S0009-2541(97)00078-8.

Nelson, G.J., Pufahl, P.K., and Hiatt, E.E., 2010, Paleoceanographic constraints on Precambrian phosphorite accumulation, Baraga Group, Michigan, USA: Sedimentary Geology, v. 226, no. 1-4, p. 9–21, doi:10.1016/j.sedgeo.2010.02.001.

Papineau, D., 2010, Global biogeochemical changes at both ends of the Proterozoic: Insights from phosphorites: Astrobiology, v. 10, no. 2, p. 165–181, doi:10.1089/ast.2009.0360.

Papineau, D., Purohit, R., Fogel, M.L., and Shields-Zhou, G.A., 2013, High phosphate availability as a possible cause for massive cyanobacterial production of oxygen in the Paleoproterozoic atmosphere: Earth and Planetary Science Letters, v. 362, p. 225–236, doi:10.1016/j.epsl.2012.11.050.

Pašava, J., Frimmel, H., Taiyi, L., Koubová, M., and Karel, K., 2010, Extreme PGE concentrations in lower Cambrian acid tuff layer from the Kunyang phosphate deposit, Yunnan Province, South China—Possible PGE source for lower Cambrian Mo-Ni- polyelement ore beds: Economic Geology and the Bulletin of the Society of Economic Geologists, v. 105, no. 6, p. 1047–1056, doi:10.2113/econgeo.105.6.1047.

Pi, D.H., Liu, C.Q., Shields-Zhou, G.A., and Jiang, S.Y., 2013, Trace and rare earth element geochemistry of black shale and kerogen in the early Cambrian Niutitang Formation in Guizhou Province, South China: Constraints for redox environments and origin of metal enrichments: Precambrian Research, v. 225, p. 218–229, doi:10.1016/j.precamres.2011.07.004.

Planavsky, N.J., Rouxel, O.J., Bekker, A., Lalonde, S.V., Konhauser, K.O., Reinhard, C.T., and Lyons, T.W., 2010, The evolution of the marine phosphate reservoir: Nature, v. 467, no. 7319, p. 1088–1090, doi:10.1038/nature09485.

Prasad, M., Saxena, S., and Amritphale, S.S., 2002, Adsorption models for sorption of lead and zinc on francolite mineral: Industrial & Engineering Chemistry Research, v. 41, no. 1, p. 105–111, doi:10.1021/ie0102302.

Pufahl, P.K., and Grimm, K.A., 2003, Coated phosphate grains: Proxy for physical, chemical, and ecological changes in seawater: Geology, v. 31, no. 9, p. 801–804, doi:10.1130/G19658.1.

Riding, R., 2006, Cyanobacterial calcification, carbon dioxide concentrating mechanisms, and Proterozoic–Cambrian changes in atmospheric composition: Geobiology, v. 4, no. 4, p. 299–316, doi:10.1111/j.1472-4669.2006.00087.x.

Salama, W., El-Kammar, A., Saunders, M., Morsy, R., and Kong, C., 2015, Microbial pathways and palaeoenvironmental conditions involved in the formation of phosphorite grains, Safaga District, Egypt: Sedimentary Geology, v. 325, p. 41–58, doi:10.1016/j.sedgeo.2015.05.004.

Schroder, S., and Grotzinger, J.P., 2007, Evidence for anoxia at the Ediacaran-Cambrian boundary: The record of redox-sensitive trace elements and rare earth elements in Oman: Journal of the Geological Society [London], v. 164, p. 175–187, doi:10.1144/0016-76492005-022.

Schulz, H.N., and Schulz, H.D., 2005, Large sulfur bacteria and the formation of phosphorite: Science, v. 307, no. 5708, p. 416–418, doi:10.1126/science.1103096.

She, Z.B., Strother, P., McMahon, G., Nittler, L.R., Wang, J.H., Zhang, J.H., Sang, L.K., Ma, C.Q., and Papineau, D., 2013, Terminal Proterozoic cyanobacterial blooms and phosphogenesis documented by the Doushantuo granular phosphorites I: In situ micro-analysis of textures and composition: Precambrian Research, v. 235, p. 20–35, doi:10.1016/j.precamres.2013.05.011.

She, Z.B., Strother, P., and Papineau, D., 2014, Terminal Proterozoic cyanobacterial blooms and phosphogenesis documented by the Doushantuo granular phosphorites II: Microbial diversity and C isotopes: Precambrian Research, v. 251, p. 62–79, doi:10.1016/j.precamres.2014.06.004.

Shields, G., and Stille, P., 2001, Diagenetic constraints on the use of cerium anomalies as palaeoseawater redox proxies: An isotopic and REE study of Cambrian phosphorites: Chemical Geology, v. 175, no. 1-2, p. 29–48, doi:10.1016/S0009-2541(00)00362-4.

Simone, L., 1980, Ooids: A review: Earth-Science Reviews, v. 16, p. 319–355, doi:10.1016/0012-8252(80)90053-7.

Soudry, D., Ehrlich, S., Yoffe, O., and Nathan, Y., 2002, Uranium oxidation state and related variations in geochemistry of phosphorites from the Negev (southern Israel): Chemical Geology, v. 189, p. 213–230, doi:10.1016/S0009-2541(02)00144-4.

Soudry, D., Nathan, Y., and Ehrlich, S., 2013, Geochemical diagenetic trends during phosphorite formation—Economic implications: The case of the Negev Campanian phosphorites, southern Israel: Sedimentology, v. 60, no. 3, p. 800–819, doi:10.1111/j.1365-3091.2012.01361.x.

Sperling, E.A., Frieder, C.A., Raman, A.V., Girguis, P.R., Levin, L.A., and Knoll, A.H., 2013, Oxygen, ecology, and the Cambrian radiation of animals: Proceedings of the National Academy of Sciences of the United States of America, v. 110, no. 33, p. 13,446–13,451, doi:10.1073/pnas.1312778110.

Steiner, M., Wallis, E., Erdtmann, B.D., Zhao, Y.L., and Yang, R.D., 2001, Submarine-hydrothermal exhalative ore layers in black shales from South China and associated fossils—Insights into a Lower Cambrian facies and bio-evolution: Palaeogeography, Palaeoclimatology, Palaeoecology, v. 169, no. 3-4, p. 165–191, doi:10.1016/S0031-0182(01)00208-5.

Swett, K., and Crowder, R.K., 1982, Primary phosphatic oolites from the Lower Cambrian of Spitsbergen: Journal of Sedimentary Petrology, v. 52, no. 2, p. 587–593.

Tay, K.S., Rahman, N.A., Abas, M.R.B., and Simoneit, B.R., 2013, Ozonation of triterpenoids: Implications for early diagenesis of biomarkers in oxic environments: Organic Geochemistry, v. 57, p. 34–40, doi:10.1016/j.orggeochem.2013.01.001.

Tribovillard, N., Algeo, T.J., Lyons, T., and Riboulleau, A., 2006, Trace metals as paleoredox and paleoproductivity proxies: An update: Chemical Geology, v. 232, no. 1–2, p. 12–32, doi:10.1016/j.chemgeo.2006.02.012.

Van Cappellen, P., and Berner, R.A., 1991, Fluorapatite crystal growth from modified seawater solutions: Geochimica et Cosmochimica Acta, v. 55, no. 5, p. 1219–1234, doi:10.1016/0016-7037(91)90302-L.

Wang, W., and Zhou, M.F., 2012, Sedimentary records of the Yangtze block (South China) and their correlation with equivalent Neoproterozoic sequences on adjacent continents: Sedimentary Geology, v. 265, p. 126–142, doi:10.1016/j.sedgeo.2012.04.003.

Wen, H.J., Carignan, J., Zhang, Y.X., Fan, H.F., Cloquet, C., and Liu, S.R., 2011, Molybdenum isotopic records across the Precambrian-Cambrian boundary: Geology, v. 39, no. 8, p. 775–778, doi:10.1130/G32055.1.

Wen, H.J., Fan, H.F., Zhang, Y.X., Cloquet, C., and Carignan, J., 2015, Reconstruction of early Cambrian ocean chemistry from Mo isotopes: Geochimica et Cosmochimica Acta, v. 164, p. 1–16, doi:10.1016/j.gca.2015.05.008.

Wille, M., Nagler, T.F., Lehmann, B., Schroder, S., and Kramers, J.D., 2008, Hydrogen sulphide release to surface waters at the Precambrian/Cambrian boundary: Nature, v. 453, no. 7196, p. 767–769, doi:10.1038/nature07072.

Xing, Y.S., and Luo, H.L., 1984, Precambrian-Cambrian boundary candidate, Meishucun, Jinning, Yunnan, China: Geological Magazine, v. 121, no. 3, p. 143–154, doi:10.1017/S0016756800028193.

Yan, D.P., Zhou, M.F., Song, H.L., Wang, X.W., and Malpas, J., 2003, Origin and tectonic significance of a Mesozoic multi-layer over-thrust system within the Yangtze block (South China): Tectonophysics, v. 361, no. 3-4, p. 239–254, doi:10.1016/S0040-1951(02)00646-7.

Yang, H., Hao, L.J., Zhao, N.R., Huang, M.J., Du, C., and Wang, Y.J., 2013, The growth process of regular radiated nanorod bundles hydroxyapatite formed by thermal aqueous solution approach: Materials Chemistry and Physics, v. 141, no. 1, p. 488–494, doi:10.1016/j.matchemphys.2013.05.048.

Yao, W.H., Li, Z.X., Li, W.X., Li, X.H., and Yang, J.H., 2014, From Rodinia to Gondwanaland: A tale of detrital zircon provenance analyses from the southern Nanhua Basin, South China: American Journal of Science, v. 314, no. 1, p. 278–313, doi:10.2475/01.2014.08.

Zhao, J.H., Zhou, M.F., Yan, D.P., Zheng, J.P., and Li, J.W., 2011, Reappraisal of the ages of Neoproterozoic strata in South China: No connection with the Grenvillian orogeny: Geology, v. 39, no. 4, p. 299–302, doi:10.1130/G31701.1.

Zhou, C., and Jiang, S.-Y., 2009, Palaeoceanographic redox environments for the Lower Cambrian Hetang Formation in South China: Evidence from pyrite framboids, redox sensitive trace elements, and sponge biota occurrence: Palaeogeography, Palaeoclimatology, Palaeoecology, v. 271, no. 3, p. 279–286, doi:10.1016/j.palaeo.2008.10.024.

Zhou, M.Z., Luo, T.Y., Liu, S.R., Qian, Z.K., and Xing, L.C., 2013, SHRIMP zircon age for a K-bentonite in the top of the Laobao Formation at the Pingyin section, Guizhou, South China: Science in China, ser. D, Earth Sciences, v. 56, no. 10, p. 1677–1687, doi:10.1007/s11430-013-4604-7.

Zhu, R.X., Li, X.H., Hou, X.G., Pan, Y.X., Wang, F., Deng, C.L., and He, H.Y., 2009, SIMS U-Pb zircon age of a tuff layer in the Meishucun section, Yunnan, southwest China: Constraint on the age of the Precambrian-Cambrian boundary: Science in China, ser. D, Earth Sciences, v. 52, no. 9, p. 1385–1392.

Science Editor: Aaron J. Cavosie
Associate Editor: Greg Druschel

Manuscript Received 12 June 2016
Revised Manuscript Received 23 March 2017
Manuscript Accepted 5 May 2017

Printed in the USA